Morphometry of Hepatic Neoplasms and Altered Foci in the Mummichog, *Fundulus heteroclitus*

Cynthia B. Stine,[1] David L. Smith,[2] Wolfgang K. Vogelbein,[3] John C. Harshbarger,[4]
Prabhakar R. Gudla,[5] Michael M. Lipsky,[6] and Andrew S. Kane[1]

[1]*University of Maryland College Park, Department of Veterinary Medicine, Aquatic Pathobiology Laboratory,*
College Park, Maryland, USA
[2]*University of Maryland School of Medicine, Department of Epidemiology and Preventive Medicine, Baltimore, Maryland, USA*
[3]*Virginia Institute of Marine Science, College of William & Mary, Gloucester Point, Virginia, USA*
[4]*Department of Pathology, George Washington University Medical Center, Washington, DC, USA*
[5]*University of Maryland College Park, Department of Biological Resources Engineering, College Park, Maryland, USA, and*
[6]*University of Maryland School of Medicine, Department of Pathology, Baltimore, Maryland, USA*

ABSTRACT

The goal of this study was to intensively sample a small number of livers from a population of mummichog exposed to PAH-contaminated sediments and evaluate them for lesion pathology, distribution, shape, and volume, and the number of histological sections needed to adequately describe the extent of various lesions. Volumetric data for each lesion type from each step section was derived from digitized section images. The total number of hepatic alterations ranged from 10–125 per fish. Alterations included: eosinophilic, basophilic, and clear cell foci; hepatocellular carcinomas; hemangiopericytomas; and cholangiomas. Lesion volumes ranged from 0.00012–64 mm^3 and represented 0.21%–67% of total liver volume. There was a tendency for the lesions to be more dorsal-ventrally compressed than spherical or ropelike when observed from longitudinal sections. Periodic subsampling of the data indicated that, on average, 6 evenly spaced, longitudinal histological sections were required to accurately estimate lesion volume and extent in our model population. These data provide a formulation for histological sampling techniques and methodological support for piscine and other cancer study models that observe lesion volume changes over time. Further, this study fosters the development of early quantitative endpoints, rather than using a large number of animals and waiting for tumor progression or death to occur.

Keywords.   Cancer; mummichog; lesion volume; liver; morphometry; neoplasia; PAH (polycyclic aromatic hydrocarbons); stereology.

INTRODUCTION

Histopathology is a primary tool for evaluating the presence, extent, and presentation of neoplastic lesions and alterations. In a variety of carcinogenesis studies using small animal models, it is common to evaluate organs of interest using 1 or 2 histologic slides of relevant tissues (Pitot et al., 1980; Xu et al., 1990; Hanigan et al., 1993). However, the use of multiple histologic slides may prove valuable, as illustrated by Eustis et al. (1994) in evaluating renal neoplasms in experimentally exposed rats. Studies of the mummichog (*Fundulus heteroclitus*) model have shown that hepatic neoplasms and other lesions associated with environmental PAH exposure may be highly variable in their presentation, distribution, and size (Vogelbein et al., 1990; Stine, 2001). Therefore, we were interested in determining a statistically relevant number of histologic sections per specimen needed to accurately reflect changes in the entire organ. Previous studies have used stereology, a method that enables 3D-evaluations to be extrapolated from 2D-observations, to determine effects of cancer promoting agents, determine the effects of sex and age on hepatocarcinogenesis, and validate biopsy specimens (Pitot et al., 1980; Xu et al., 1990; Coward and Bromage, 2001). Other stereological methods, e.g., disector techniques (West, 1993; Charleston et al., 2003), are efficient

to count specific structures or cells within relatively large tissue domains. However, these techniques do not facilitate shape, area, distribution, or volume estimates. In this study, we used stereology to evaluate foci of cellular alteration and neoplastic lesion volume, tissue distribution, shape, and an adequate histological sampling strategy, using mummichog collected from a PAH-contaminated site. Lastly, a 3D-volume of liver from longitudinally sectioned slices from 1 case was reconstructed to demonstrate and compare the observational effect of varying section orientation.

MATERIALS AND METHODS

Fish and Livers

Adult mummichog were collected in minnow traps from the creosote-contaminated South Branch of the Elizabeth River that discharges via the mouth of the James River into the Virginia portion of the Chesapeake Bay. Fish were humanely euthanized by cervical translocation according to protocols approved by the University of Maryland's Animal Care and Use Committee. Whole livers were removed and fixed in 10% neutral buffered formalin (Kane, 1996). Livers were embedded in paraffin blocks and oriented to generate longitudinal histologic sections along the frontal plane (Figure 1). Sections of 5–6 μm thickness were taken every 10th slice, approximately every 60 μm, throughout the entire liver. This resulted in 42–63 sections per liver based on liver size. Sections were stained with hematoxylin and eosin (Profet et al., 1992).

All sections of 6 livers were reviewed for pathological alterations. Frank neoplasms and basophilic and eosinophilic
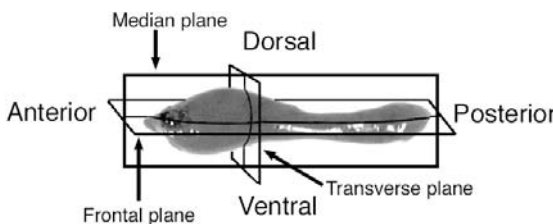

FIGURE 1.—Orientation of the mummichog liver. Longitudinal sections were generated along the frontal plane of the organ. Sectioning began at the ventral edge of the liver (low numbered slices) and continued dorsally.

foci were characterized according to Boorman et al. (1997). Clear cell foci were characterized as having clear cytoplasm resembling fat droplets or glycogen (Vogelbein et al., 1990). Sections were photographed with a Nikon-Fuji DX digital camera at low magnification on an Olympus BH microscope. Each lesion type from each digital slice image was carefully outlined and blackened using Adobe Photoshop software. Accuracy of this procedure was aided by the use of side-by-side comparison with higher magnification microscopic observations. The blackened images were then imported into NIH Image ⟨http://rsb.info.nih.gov/nih-image⟩ software for liver area and the different lesion area analyses. Area data were compiled in spreadsheets, organized by fish case number and lesion type, and presented graphically using Microsoft Excel software.

Stereology

Stereology was applied to the liver and lesion area data. These data were compiled in spreadsheets and graphed by slice number to depict the centroid (i.e., the 3D-center point) of each lesion. Lesion centroids were discerned by first observing the fraction of the total area occurring on each slide using the following equation: $P(x) = A_x / \Sigma A_x$, where A_x is the observed area (in the xyplane) of the lesion on slide x. The centroid of each lesion was then determined using the equation: $c = \Sigma xP(x)$, where c is the position of the centroid in the z-axis (i.e., the slice number that the center of the lesion occurs). Lesion centroid data were plotted in histograms to provide a visual representation of lesion distribution throughout each of the livers in the z-plane.

Total lesion area for each liver was determined by summing the estimated areas of individual lesions for all lesion types. The estimated volume of each lesion was derived by the equation: $V = \Sigma_x(A_x \Delta_x)$, where V is the volume of a lesion in a liver, x is the slice number, A_x is the area (in the xy-plane) of the lesion on the xth slide, and Δ_x is the distance between slices. Lesion volume equals the sum of the area occupied by a lesion on slice x multiplied by the distance between slices for all the slices on which the lesion appears. Total liver volume was calculated using the same equation. The observed estimate of total lesion volume for the entire liver (M) was derived from summing the individual lesion volume estimates: $M = \Sigma_i V_i$, where V_i is the volume for each lesion.

Lesion shapes were evaluated by graphing lesion volumes versus a theoretical sphere. Lesion volume data were plotted against the number of slices that each lesion intersected. The resulting data points were compared to a line representing a theoretical sphere of increasing volume. This sphere line was determined by the following logic: a lesion intersecting 1 slice was assumed to have a diameter of Δ_x and a radius of $0.5\Delta_x$. In our case, Δ_x equals 60 μm, so using the formula for the volume of a sphere, $\frac{4}{3}\pi r^2$, a volume of 0.00011 mm^2 was obtained for a lesion intersecting one slice. Lesions falling above the sphere regression line were considered more pancake-like or dorsal-ventrally compressed when observed in our longitudinal sectioning method (refer to Figure 1), whereas lesions falling below the line were considered more ropelike.

A periodic subsampling method was applied to estimate lesion areas based on fewer and fewer observations, compared to all slice observations. Total lesion volume estimates, based on all step sections were compared to total lesion volume estimates based on fewer than the available number of sections. For each lesion type in each fish, a volume estimate was obtained by summing the area of all lesions of that type on all available sections. Sections were systematically subsampled at regular intervals to obtain volume estimates based on a subset of the total data. For example, a volume estimate was obtained by summing the lesion area from every other slice and multiplying the result by 2 to get an estimated volume of the lesions that was comparable to the original estimated volume. This was done twice, with 1 sample starting at section 1, the other starting at section 2, giving 2 estimates of lesion volume based on half the number of available slices. Subsequently, the slices could be observed 3 times, starting at the 1st, 2nd, and 3rd slices, and so forth. This procedure was repeated until estimates were obtained from only 1 section. For each fish, volume estimates were plotted as a function of the number of sections used to generate the volume estimate, V. These estimates, based on the subsampling procedure, were compared to the estimated total liver lesion volume (M). Data derived from subsampling were visualized using box plots, generated with "R" software (The R Foundation for Statistical Computing, Vienna University of Technology, Vienna, Austria; ⟨http://www.r-project.org⟩, version 1.3.0).

3D-Reconstruction

To demonstrate lesion observations from multiple sectioning perspectives, 1 liver (case 6) and its lesions were reconstructed volumetrically from the digital section images. The reconstruction was performed using MATLAB software (The Mathworks, Inc., Natick, MA 01760; ⟨http://www.mathworks.com⟩, version 6.1). To account for section deformations such as rotational and translational offsets, and independent amounts of scaling and/or nonlinear deformation due to cutting, folding, specimen tilt, and optical distortion, a set of transformations $\{T_i\}$ was generated such that objects in each section were in alignment throughout the liver volume (Stevens and Trogadis, 1984). Each transformation is represented by the functions:

$$u = a_0 f_0(x, y) + a_1 f_1(x, y) + a_2 f_2(x, y) + K + a_n f_n(x, y)$$
$$v = b_0 f_0(x, y) + b_1 f_1(x, y) + b_2 f_2(x, y) + K + b_n f_n(x, y)$$

where (u, v) is a pixel of the original image, (x, y) is a pixel of the untransformed image and bivariate polynomials were

chosen as the basis functions $\{f_j(x, y)\}$:

$$\{f_0(x, y) = 1, f_1(x, y) = x, f_2(x, y) = y, f_3(x, y)$$
$$= xy, f_4(x, y) = x^2, f_5(x, y) = y^2\}.$$

The real-valued parameters $\{a_j\}$, $\{b_j\}$, $j = 0 \ldots 5$, specify the particular transformation for each section and were determined from a set of point correspondences (Umeyama, 1991; Lawrence, 1992). The internal lesion and liver volume data were superimposed on a gross liver image that was adjusted to fit the reconstructed liver surface based on the calculated isosurfaces on the aligned stack of longitudinal section images.

RESULTS

Fish and Liver Descriptions

Mummichog analyzed in this study were externally unremarkable. The total length of the 6 fish ranged from 60–97 mm and weights ranged from 4–11 g. The liver weights ranged from 64–314 mg and ranged in color from dark brown to light tan. Five of the 6 livers had grossly visible nodules. The nodules ranged in diameter from 1–10 mm and were clear, white, or dark tan in color. Histological step sectioning yielded between 42 and 63 sections, depending on the thickness of the liver.

By histologic analysis, 321 nonreactive, proliferative lesions in the neoplastic sequence were observed from the 6 fish. These included eosinophilic, basophilic, and clear cell foci of hepatocellular alteration; hepatocellular carcinomas; cholangiomas; and hemangiopericytomas (Vogelbein et al., 1990; Boorman et al., 1997). Reactive lesions, such as chronic inflammation and macrophage aggregates, were also observed but not analyzed in the present study. There were no metazoan or protozoan parasites in the livers.

Qualitative Pathology Observations

The eosinophilic, basophilic, and clear cell foci of hepatocellular alteration were small populations of tinctorially altered hepatocytes with minimal cytologic abnormalities. Characteristic lesions are shown in Figure 2. A hemangiopericytoma, observed in case 2, was a large mass of whorling, fusiform, spindle cells around capillary-like structures (Figures 2D–E) similar to those observed by Boorman et al. (1997). The invading tumor occupied 26% of the liver parenchyma. A large, variably differentiated hepatocellular carcinoma in case 4 contained necrotic and fibrotic areas. Some tumor cells had a high nuclear:cytoplasm ratio and a high degree of cellular and nuclear pleomorphism. The tumor had a relatively smooth border, even though it replaced approximately two-thirds of the normal liver (Figures 2F–G). Cholangiomas, comprised of irregular ductular structures with thick, periductular fibrous capsules, were observed in cases 5 and 6. The largest cholangioma is illustrated in Figures 2H–I.

Quantitative Pathology Observations

All fish had eosinophilic foci, and 4 out of 6 had basophilic foci. Four of 6 fish also had clear cell foci. Eosinophilic foci were the most numerous lesions within individual livers except in 1 case where clear cell foci were most numerous. Clear cell foci were the next most numerous type of lesion.

When liver lesion area was not dominated by a large central neoplasm, smaller altered foci had a tendency to be relatively homogeneously distributed throughout the liver. However, empirical observations indicated that the frequency distribution of smaller lesions was affected by the presence of larger lesions. This was visualized by comparing lesion area data and lesion frequency data (Figure 3). Lesion centroids were clumped ventrally in 3 cases where there was a relatively large lesion (i.e., hemangiopericytoma, hepatocellular carcinoma, or cholangioma) present.

Volumetric Data

Volumetric data derived from this study are summarized in Table 1. Livers ranged in volume from 26.08–95.60 mm^3, the lesions ranged from 0.00012–63.87 mm^3. Lesions within each liver accounted for 0.21% to 67.36% of the whole liver volumes.

Frank Neoplasms: Large neoplastic lesions, when present, dominated total liver volume and lesion volume. For example, the hemangiopericytoma case (case 2) accounted for 26.4% of total liver volume and 91.8% of lesion volume. Also, the hepatocellular carcinoma in case 4 accounted for 66.8% of the whole liver volume and accounted for 99.2% of lesion volume.

Foci of Cellular Alteration: Altered foci accounted for 100% of lesion volume in 2 cases without frank neoplasms (cases 1 and 3). In case 2, altered foci accounted for 3.2% of liver volume not attributed to the hemangiopericytoma. In case 4, altered foci accounted for 1.7% of liver volume not attributed to the hepatocellular carcinoma. In case 5, eosinophilic foci accounted for 98.5% of total lesion volume and 9.5% of total liver volume. One particular focus spanned 18 slices. In case 6, altered foci accounted for 1.8% of liver volume not attributed to the cholangioma.

Shapes of Lesions: The shapes of the lesions observed in this study were variable, and there was a tendency for the lesions to be more pancake-like than spherical or ropelike when viewed from longitudinal, frontal slices (Figure 4). Extreme dorsal-ventral compression of a few lesions (eosinophilic and basophilic foci) was found in 3 livers.

Periodic Subsampling

The total estimated volumes of lesion types and total lesion volume for each liver, based on fewer than the total number of available slices, were visualized using box plots (Figure 5). These data indicated variability between cases in the number of histological sections required to estimate lesion volumes in each liver. An acceptable estimate of total lesion volume was defined when at least 50% of the sample data fell within the standard error of the true mean based on the sample mean.

General trends followed intuition: discerning numerous large lesions would require less intensive sampling, whereas the fewer smaller lesions would require more intensive sampling. The numbers of sections required for acceptable estimates of individual cases are presented in the Table 2. Based on our acceptable estimate criteria, on average, 6 sections
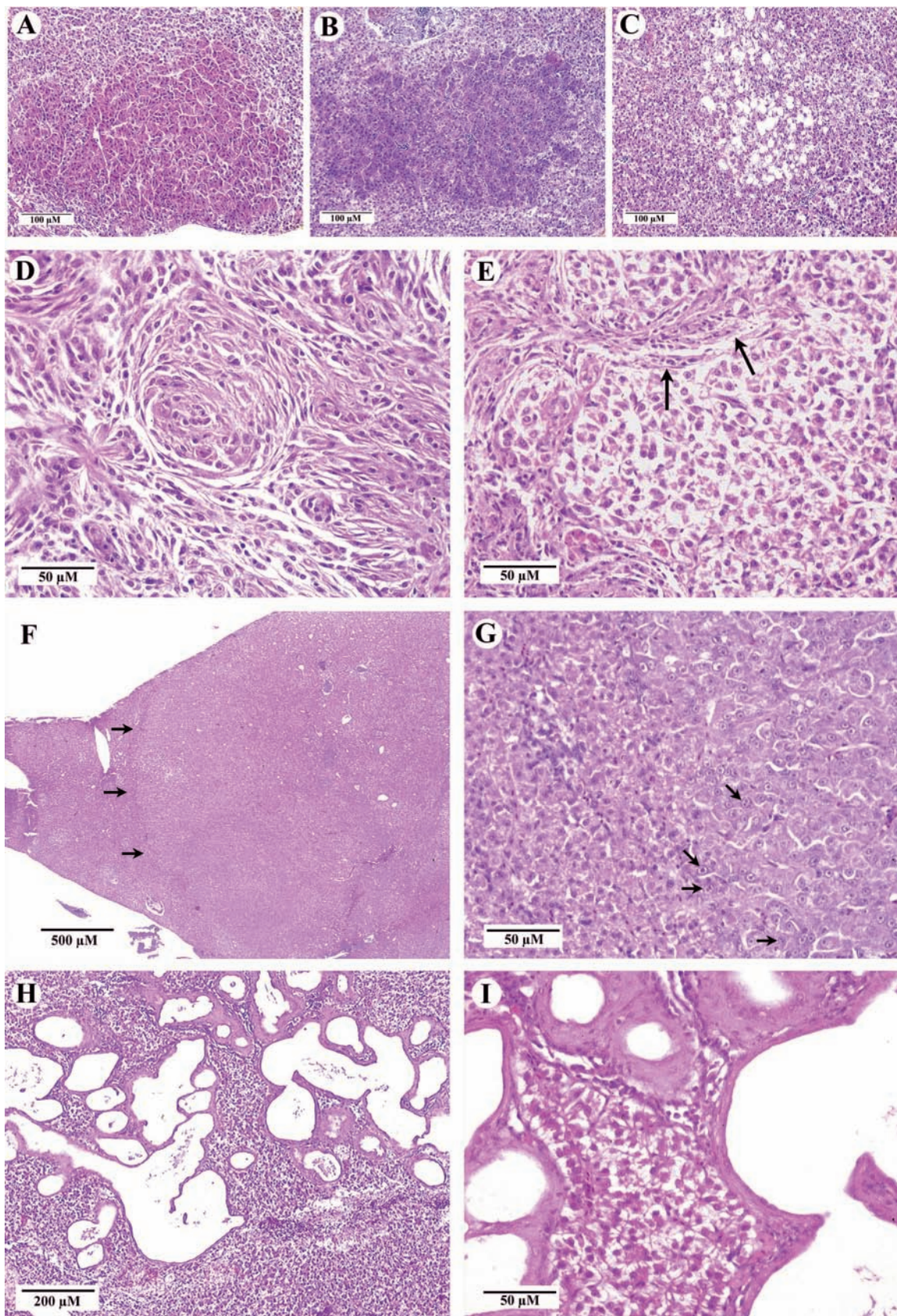
FIGURE 2.—Examples of hepatic lesions observed from mummichog collected from the South branch of the Elizabeth River. Observations included: eosinophilic foci (A), basophilic foci (B), clear cell foci (C), and neoplasms. Neoplastic lesions included: a hemangiopericytoma comprised of spindle-shaped cells whorled around a central capillary (D), portions of which had invasive edges (E); a large hepatocellular carcinoma (left margin indicated by arrows) (F). At higher magnification the hepatocellular carcinoma (with normal tissue on the left) consisted of highly pleomorphic cells with nuclear atypia; many nuclei had multiple nucleoli (arrows) (G). An early cholangioma was characterized by ductular structures that mimicked the biliary tissue of origin (H and I).
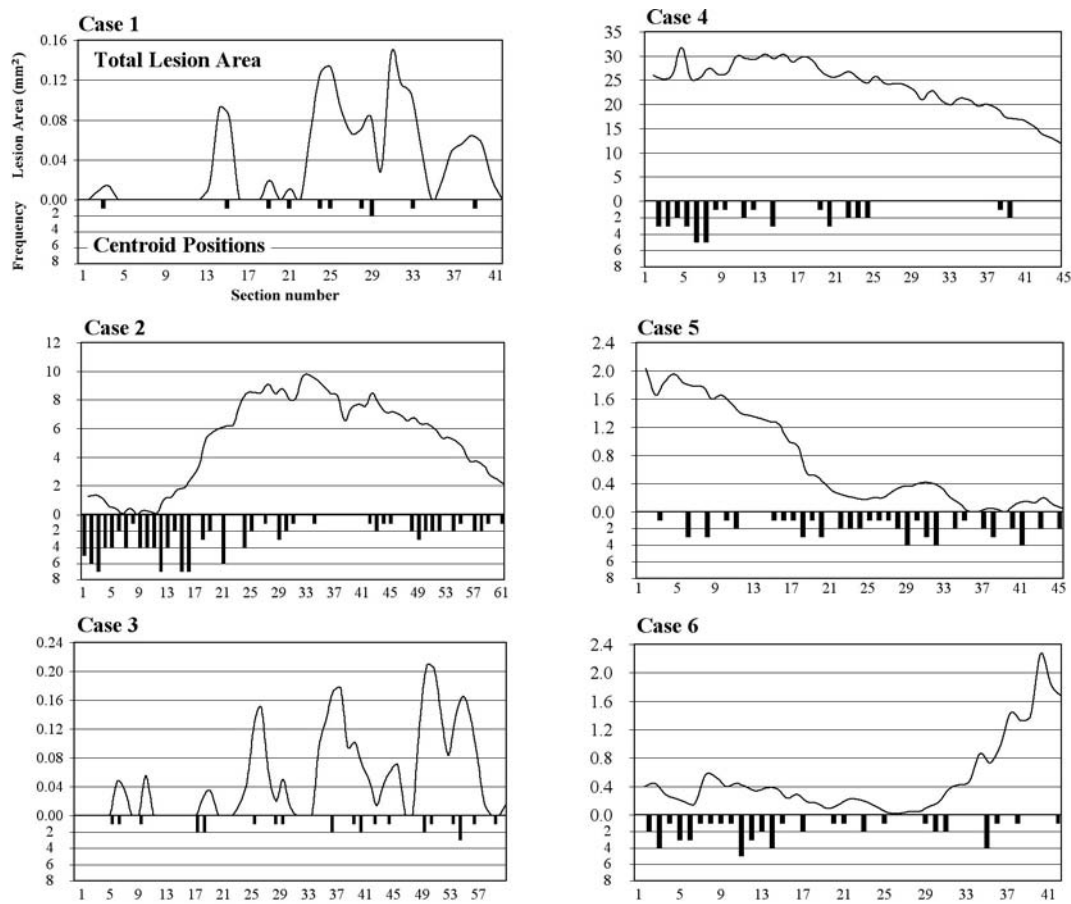
FIGURE 3.—Lesion areas and centroid positions of hepatic alterations for the 6 mummichog livers sampled in this study. Each case depicts total lesion area in the top of each panel (note that scale varies) and position of the lesion centroids in the bottom of each panel. Lower section numbers (x-axes) represent the ventral portion of the liver while higher section numbers represent the dorsal portion of the liver. Cases 1, 3, and 5 did not have neoplasms; case 5 had a large, ventrally located, eosinophilic focus. Case 2 had a hemangiopericytoma that spanned the dorsal two-thirds of the liver. Case 4 had a hepatocellular carcinoma throughout all sections. Case 6 had multiple, dorsal cholangiomas.

were required to discern lesion extent in our population of mummichog livers.

3D-Reconstruction

Lesion data from 1 case were digitally reconstructed, and a cutaway illustration was rendered to show the relative volume and location of the lesions within the 3D-liver architecture (Figure 6). This reconstruction illustrates how lesion observations may vary depending on plane of section (tissue orientation), as well as the specific sections observed.

DISCUSSION

Sampling a population to assess the impact of exposure to a carcinogenic chemical requires a basic understanding of the distribution of exposure-associated lesions within a liver and the distribution of these lesions across a population. Early efforts using stereology to estimate histological lesion volumes (Pitot et al., 1980; Xu et al., 1990; Hanigan et al., 1993) provided an innovative approach to estimate lesion extent. However, more recent efforts by Eustis et al. (1994) and Mazonakis et al. (2002), using renal histopathology and hepatic MRI, respectively, show that observations from multiple

TABLE 1.—Summary of hepatic lesion data from 6 mummichog.

Lesion type	Range of number observed*	Mean volume (±S.D.) (mm^3)	Mean cumulative volume (±S.E.) (mm^3)	Range of percent whole
Eosinophilic focus	2–75	0.01 ± 0.012	0.6 ± 0.78	0.01–9.5
Basophilic focus	2–20	0.04 ± 0.014	0.2 ± 0.20	0.04–0.5
Clear cell focus	2–36	0.002 ± 0.0021	0.05 ± 0.065	0.004–0.21
Granuloma	1	0.02	0.02	0.05
Hepatocellular carcinoma	1	64	64	67
Hemangiopericytoma	1	17	17	26
Cholangioma	1–4	0.1 ± 0.12	0.4 ± 0.56	0.12–3.1
Total lesion	10–125	—	10 ± 26	0.21–67
Total liver	—	—	50 ± 28	100

Range of lesion numbers observed per case (∗) is based on centroid counts, not multiple observations of same lesion in different sections.

TABLE 2.—Breakdown of percent lesion volumes and longitudinal section requirement estimates for each case by lesion type.

Case #	Lesion type	% Total lesion volume	% Liver volume	No. sections required for 50% accuracy	No. sections required for 95% accuracy
1	Eosinophilic	71	0.1	4	7
	Basophilic	29	0.04		
2	Hemangiopericytoma	92	26	3	3
	Eosinophilic	7	2		
	Basophilic	0.8	0.2		
	Clear cell	0.7	0.2		
3	Eosinophilic	99	0.4	9	15
	Clear cell	1	0.004		
4	Hepatocellular carcinoma	99	67	7	7
	Eosinophilic	0.02	0.01		
	Basophilic	0.7	0.5		
	Clear cell	0.1	0.04		
	Cholangioma	1	0.1	5	5
5	Eosinophilic	98	9		
	Clear cell	0.2	0.02		
	Choangioma	64	3	7	7
6	Eosinophilic	28	1		
	Basophilic	7	0.3		
			Mean no. slices required:	6	7

The number of sections required for volume "accurate" volume estimates is based on 50 or 95% of the periodic subsampling procedure volume estimates falling within 1 standard deviation of the mean volume estimate when all liver sections are observed (see example box plot, Figure 5). Note that the number of sections required to achieve 50 and 95% confidence is similar when a large volume (i.e., >1% liver volume) lesion occurs, such as in cases 2, 4, 5, and 6. Interestingly, in case 5 this is not due to the cholangioma, but a large eosinophilic focus.
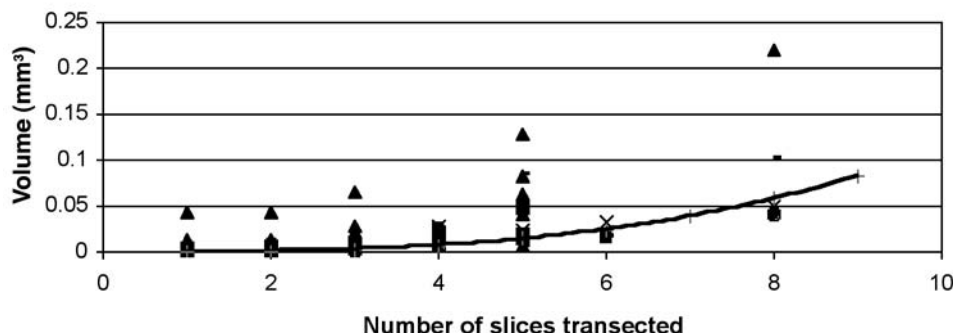
Shape of Lesions

FIGURE 4.—Shape of lesions from all 6 livers, all lesion types. The regression curve represents the volume of a theoretical sphere with increasing diameter. Lesions falling above the line were more pancake-like in longitudinal sections, i.e., compressed dorsal-ventrally; lesions falling below the line were more ropelike in longitudinal sections, i.e., compressed anterior-posteriorly. There was a tendency for lesions to be dorsal-ventrally compressed when viewed in longitudinal, frontal plane sections.
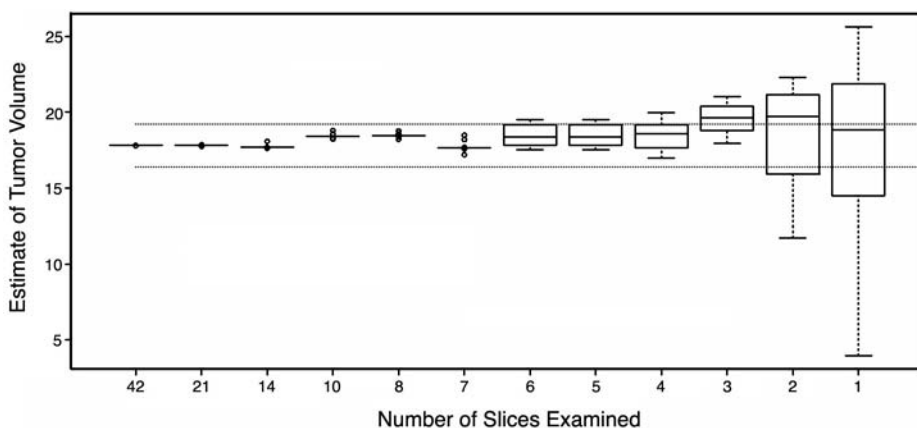

FIGURE 5.—Box plot of volume data for case 1 (typical of all cases) estimating lesion volume based on the summation of area data (mm^3). Individual estimate points are shown as open circles; if the points fall too closely together to distinguish, a box replaced the circles, with the upper and lower hinges of the box representing the 25th and 75th quartile of the sample data. The extended arms represent the 5th and 95th twentieths of the sample data. The middle horizontal lines for each slice category are the medians of the volume estimates for that category. An acceptable estimate of lesion volume occurred when the box fell within the standard errors of the true mean based on the sample mean (i.e., the dotted horizontal lines). In the above example, at least 4 sections were necessary to generate an "acceptable estimate" of the true lesion volume.
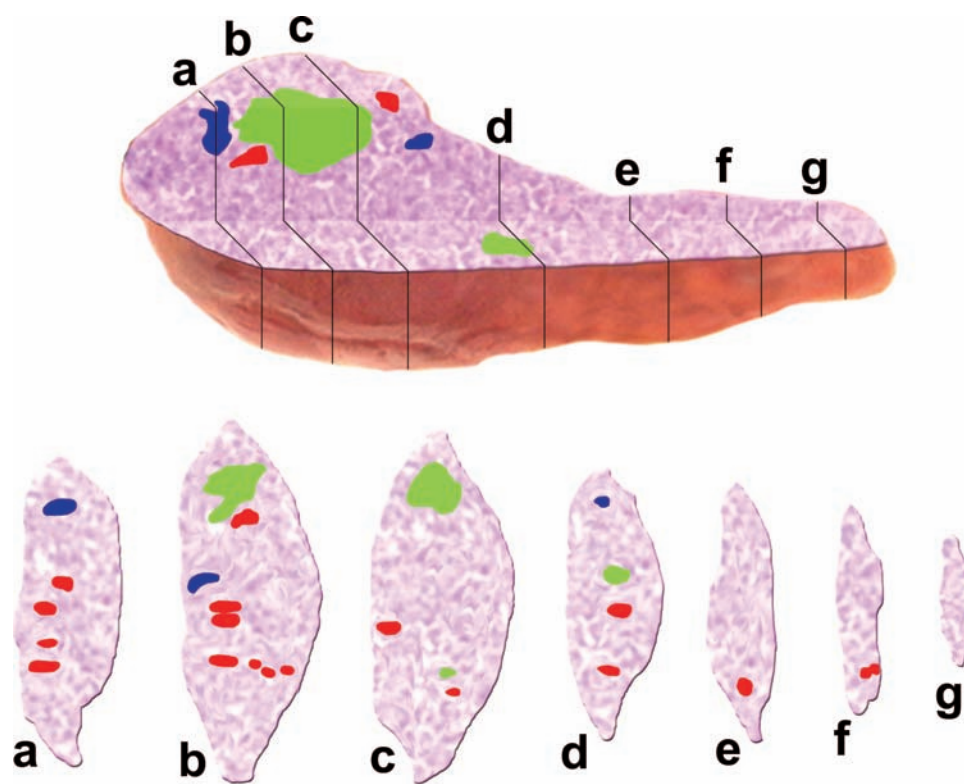
FIGURE 6.—Digitally reconstructed liver lesions overlaid on a proportionally sized liver cutaway diagram (above), and on representative cross-sections (below). The orientation of the liver in the upper portion of the figure is the same as in Figure 2. Red areas represent eosinophilic foci, blue areas represent basophilic foci; and green areas are cholangiomas. This illustration depicts how lesion observations vary depending on the plane of tissue sectioned and which sections are observed. For example, the visible portion of the longitudinal section observed along the horizontal cut surface (upper cutaway diagram) only contains a portion of a cholangioma. However, cross-section d, through that same lesion, also includes a basophilic focus and 2 eosinophilic foci. Observations from different cross-sections can also make a notable difference in diagnosis. For example, if only cross-sections a, e, f, and g were sampled, the observation of a marked cholangioma would be missed; if sections c, e, f, and g were sampled, multiple basophilic foci would fail to be noted. Based on statistical analyses from this study, at least 6 longitudinal tissue sections need to be observed in order to be at least 50% confident in making accurate, repeatable lesion observations.

sections can be useful for making more accurate lesion and tissue volume estimates.

Using livers subsampled from a population of mummichog with hepatic alterations, the primary goal of this study was to ask the question: How many tissue sections are needed to estimate lesion volume? We also wanted to evaluate the 3D-lesion presentation. Samples were evaluated for lesion pathology, lesion distribution, lesion shape, lesion volume, and the number of sections needed for adequate lesion extent estimation.

Pathology

The different lesion types observed in our study are similar to those observed from mummichog sampled 14 years ago and described by Vogelbein et al. (1990). Therefore, exposure to PAHs continues in this population. Based on the observations from livers in this study, 2 broad generalizations can be made: The largest hepatic lesions observed in this study were the true neoplastic lesions: the hepatocellular carcinoma in case 4 (volume = 63.87 mm^3), the hemangiopericytoma in case 2 (volume = 17.29 mm^3), and the cholangiomas of cases 6 and 5 (volumes = 0.81 mm^3 and 0.02 mm^3, respectively). The largest nonneoplasia was an eosinophilic focus

(volume = 1.25 mm^3) in case 5. Secondly, the presence of 1 lesion type in a liver did not appear to preclude the presence of another lesion type. However, it could be generalized that the presence of a large, centrally located, space occupying lesion may decrease the number of other lesions found in the slices on which the large lesion occurs. For example, the large hemangiopericytoma in case 2 was dorsal and centrally located within the liver. There was a relatively higher frequency of smaller lesions in the ventral histological sections compared with a lower lesion frequency but larger lesion area in the dorsal liver sections (where the hemangiopericytoma was observed) (Figure 3). A similar instance was observed in case 6, where a relatively higher frequency of smaller foci dominated in the ventral sections, representing a small area, while a lower frequency of larger area lesions (cholangiomas) were observed in the dorsal slices (Figure 3).

When a relatively large number of lesions were present in a liver (e.g., cases 2, 4, 5, and 6), most of the lesions, and/or lesion area, tended to predominate at either the dorsal or ventral portions of the liver (Figure 3). In case 2, this may have been associated with the centrally located hemangiopericytoma. The reason for this tendency is unclear. It is unlikely that regional blood flow kinetics within the fish liver allow metabolically reactive toxins to reside longer in

the peripheries because fish livers are not lobed (Hinton and Couch, 1998). The apparent skewedness of lesion frequency to the ventral portion of the livers may be accounted for, in large part, merely by the increased liver area in those sections. The ventral sections included both anterior and posterior portions of the liver while the dorsal slices contain only anterior portions (refer to Figure 1). Liver area in the dorsal-most sections was as little as one-third that of the ventral slices. The limited sample number (n = 6) did not allow for mathematical manipulation to compensate for this discrepancy of liver area with any accuracy, nor to address differences associated with animal age, size, or gender. Although data from the present study do not support (or refute) lesion distribution or volume relationships associated with animal age, size, or gender, it is possible that trends in lesion type may vary with these factors (e.g., Cooke and Hinton, 1999).

Stereology

Preparation artifact may have contributed to the observed variations in shape of hepatic lesions in this study. Pugh et al. (1983) found a 16% horizontal expansion of paraffin sections when they were placed on a water bath during processing. Lesions observed in this study tended to be wider anterior-posterior, as well as laterally, and as viewed by our sampling techniques, with the broad axes of the lesions falling along the longitudinal transects of the livers. This is consistent with the observations of Pugh et al. (1983). However, some lesions had extreme dorsal-ventral compression (i.e., as observed in case 2) that were likely not due to processing artifact. This supports biological intuition, that many lesions may not be regular or spherical, particularly those of an infiltrative nature.

In general, it stands to reason that smaller lesions would be less likely to be missed when larger areas are available for observation (e.g., longitudinal sections). Further, multiple larger sections that provide a better transect of the tissue will likely yield greater accuracy and relational (i.e., diffuse, focal, multifocal) information than multiple, smaller sections.

Taking histological sections from different planes of orientation may give different results and conclusions. For example, observations from the 7 cross-sectional slices in Figure 6 appears to underestimate total liver lesion area, whereas observing 7 longitudinal sections will, on average, provide an acceptable estimate of lesion area (Table 2). Therefore, histological observations from a relatively small liver, such as from a mummichog, require a greater number of cross-sectional slices than longitudinal slices to observe the same exposure-related pathologies.

Our data indicated that, for our model, an average of 6 sections should be observed by a pathologist to provide an acceptable estimate of total lesion volume (i.e., 50% of the lesion volume estimates fall within 1 standard error of the true mean based on the sample mean). Interestingly, increasing the average number of slices observed to 7 would allow for 95% of the lesion volume estimates to be included (Table 2). If a liver had a large alteration, the number of sections required for a 95% estimate remained similar as the number of slices required for a 50% estimate. In the absence of a large (>1% of the liver volume) focus, the number of slices required for a 95% estimate almost doubled that of the number of slices required for a 50% estimate. Therefore, because smaller le-

sions are more easily missed during sampling, taking more sections reveals a pattern of more lesions.

Based on our findings we can recommend some "rules of thumb." In general, large or uniformly distributed lesions are extremely likely to be found by examining a single cross-section of the liver, but adequate estimates of the total lesion volume requires observations from at least 6 sections. However, the number of evenly spaced sections needed for good volume estimates may vary with different organ or tissue sizes. Interestingly, Mazonakis et al. (2002) determined that 5–8 MRI slices from human liver, an organ that is large, multilobed, and has an irregular shape, were sufficient to adequately describe whole organ volume.

Volume estimates from stereology are based on the assumptions that lesions are spherical and homogeneously dispersed. The lesions in hepatic tissue from our model fish population tended to not be spherical and were not homogeneously dispersed. Therefore our periodic subsampling method may result in a better estimate of total lesion volume than current stereological methods. For pathologists conducting laboratory studies, a pilot study may be advisable to discern the minimum number of sections required to estimate lesion volume in the particular model proposed. Further, care must be taken when consistently defining lesion boundaries, particularly since the edges of some lesions or foci may not be well demarcated.

Data obtained using a fish model in this study were from an intensively sampled, small population subsample. Although certain trends emerged from the data, and they appear to reflect the sampled group, the quantitated results had relatively high variability. Regardless, the data generated several useful morphometric analyses and a 3D-reconstruction. This study provides diagnosticians with data and imagery to support key histological constructs:

(a) cancerous and precancerous lesions are not homogeneously distributed or spherical in shape;
(b) the presence of 1 lesion type may influence the extent and distribution of other lesions;
(c) multiple sections are needed to confidently assess the presence and extent of cancerous lesions; and
(d) tissues sectioned in different planes (cross-sectional, longitudinal, tangential, etc.), and observations from different sections will generate different lesion observations and conclusions.

Using a statistical approach, exemplified in our study, pathologists can determine how many sectional observations are actually necessary to confidently make inference regarding the extent (minimal, mild, moderate, marked, severe) and presentation (focal, multifocal, diffuse) of lesions. Application of stereological methods, such as those described herein, can provide useful baseline data for future sampling efforts. Lastly, these efforts support cancer studies and other research of progressive diseases, by fostering early quantitative endpoints, rather than using a larger number of animals and waiting for tumor progression or death to occur.

REFERENCES

Boorman, G. A., Botts, S., Bunton, T. E., Fournie, J. W., Harshbarger, J. C., Hawkins, W. E., Hinton, D. E., Jokinen, M. P., Okihiro, M. S., and Wolfe, M. J. (1997). Diagnostic criteria for degenerative, inflammatory, proliferative nonneoplastic and neoplastic liver lesions in medaka (*Oryzias latipes*):

Consensus of a National Toxicology Program Pathology Working Group. *Toxicol Pathol* **25**, 202–10.

Charleston, L. B., Thyer, A. C., Klein, N. A., Soules, M. R., and Charleston, J. S. (2003). An improved method for the production of slides from oversized samples of glycol methacrylate-embedded tissues: application for optical dissector based stereology. *J Histotechnol* **26**, 49–52.

Cooke, J. B., and Hinton, D. E. (1999). Promotion of 17ß-estradiol and ß–hexachlorocyclohexane of hepatocellular tumors in medaka, *Oryzias latipes*. *Aquat Toxicol* **45**, 127–45.

Coward, K., and Bromage, N. R. (2001). Stereological validation of ovarian biopsy as a means of investigating ovarian condition in broodstock tilapia in vivo. *Aquaculture* **195**, 183–8.

Eustis, S. L., Hailey, J. R., Boorman, G. A., and Haseman, J. K. (1994). The utility of multiple-section sampling in the histopathological evaluation of the kidney for carcinogenicity studies. *Toxicol Pathol* **22**, 457–72.

Hanigan, M. H., Winkler, M. L., and Drinkwater, N. R. (1993). Induction of three histochemically distinct populations of hepatic foci in C57BL/6J mice. *Carcinogenesis* **14**, 1035–40.

Hinton, D. E., and Couch, J. A. (1998). Architectural pattern, tissues and cellular morphology in livers of fishes: relationship to experimentally-induced neoplastic responses. In: *Fish Ecotoxicology*, T. Braunbeck, D. E. Hinton, and B. Streit (eds). Birkhauser Verlag, Basel, Switzerland, pp. 141–64.

Kane, A. S., Ed. (1996). *Fish Guts: A Multimedia Guide to the Art and Science of Fish Anatomy, Health, and Necropsy*. APC Press, Baltimore, MD.

Lawrence, M. C. (1992). Least-squares method of alignment using markers. In: J. Frank, editor, *Electron Tomography: Three-Dimensional Imaging with the Transmission Electron Microscope*, Plenum Press, New York, pp. 197–204.

Mazonakis, M., Damilakis, J., Maris, T., Prassopoulos, P., and Gourtsoyiannis, N. (2002). Comparison of two volumetric techniques for estimating liver volume using magnetic resonance imaging. *J Magn Reson Imaging* **15**, 557–63.

Pitot, H. C., Goldsworthy, T., Campbell, H. A., and Poland, A. (1980). Quantitative evaluation of the promotion by 2,3,7,8-tetrachlorodibenzo-*p*-dioxin of hepatocarcinogenesis from diethylnitrosamine. *Cancer Res* **40**, 3616–20.

Profet, E. B., Mills, B., Arrington, J. B., and Sobin, L. H. (1992). *Laboratory Methods in Histotechnology*. Armed Forces Institute of Pathology, Registry of Pathology, Washington, DC.

Pugh, T. D., King, J. H., Koen, H., Nychka, D., Chover, J., Wahba, G., He, Y., and Goldfarb, S. (1983). Reliable stereological method for estimating the number of microscopic hepatocellular foci from their transactions. *Cancer Res* **43**, 1261–8.

Stevens, J. K., and Trogadis, J. (1984). Computer-assisted reconstruction from serial electron micrographs: a tool for the systematic study of neuronal form and function. *Ad Cell Neurobiol* **5**, 341–69.

Stine, C. B. (2001). Morphometric evaluation of hepatic lesions in killifish, *Fundulus heteroclitus*, exposed to polycyclic aromatic hydrocarbons. Masters Thesis, University of Maryland at Baltimore.

Umeyama, S. (1991). Least-squares estimation of transformation parameters between two point patterns. *IEEE Trans Pattern Anal Machine Intel* **13**, 376–80.

Vogelbein, W. K., Fournie, J. W., Van Veld, P. A., and Huggett, R. J. (1990). Hepatic neoplasms in the mummichog *Fundulus heteroclitus* from a creosote-contaminated site. *Cancer Res* **50**, 5978–86.

West, M. J. (1993). New stereological methods for counting neurons. *Neurobiol Aging* **14**, 275–85.

Xu, Y. H., Campbell, H. A., Sattler, G. L., Hendrich, S., Maronpot, R., Sato, K., and Pitot, H. C. (1990). Quantitative stereological analysis of the effects of age and sex on multistage hepatocarcinogenesis in the rat by use of four cytochemical markers. *Cancer Res* **50**, 472–9.